Published in
Journal of Physics B: Atomic, Molecular and Optical Physics 29, issue 20, 4659-4673, 1996
which should be used for any reference to this work

Anisotropic magneto-optical trapping of atoms: capture efficiency and induced drift velocities

G Dudle, N Sagna, P Berthoud and P Thomann

Observatoire Cantonal, Rue de l'Observatoire 58, CH-2000 Neuchâtel, Switzerland

Abstract. An anisotropic magneto-optical trap is studied as the potential source of a continuous beam of laser-cooled atoms. Capture efficiency and cloud temperature are measured experimentally and found to be lower than in an isotropic situation with the same cooling parameters. Intensity imbalance and static magnetic field are investigated as possible extraction mechanisms. While only small drift velocities are induced by means of intensity imbalance, velocities of tens of cm s^{-1} are observed with a static magnetic field; the shape of the observed two-peaked velocity distributions is related to the average depth of local light-shift-induced potential wells.

1. Introduction

Since its first demonstration in 1987 [1], the magneto-optic trap (MOT) has become a powerful tool for producing large numbers of neutral atoms at very low temperatures. The relatively large capture velocity of the MOT makes it possible to capture an appreciable part of the low-velocity tail in the thermal velocity distribution of a vapour at ordinary temperatures, and to trap them in a volume much smaller than that determined by the laser beam diameter. Densities up to 10^{11} atoms/cm^3 and temperatures in the μK range have been reported for caesium [2–4]. Most studies of magneto-optical trapping have been devoted to 'spherical' MOTs where the magnetic field increases linearly in all directions from its zero value at the trap centre. Anti-Helmholtz coils typically produce the required field configuration, with the gradient along the coil axis being twice its value in the perpendicular directions. The trapping force in such a structure is typically four orders of magnitude larger than the atomic weight, with trap depths of a few tenths of a Kelvin. Atoms can therefore be extracted in a controlled way only after the gradient has been switched off. In many applications, however, cold atoms must be outside of the trap to be usefully probed; this implies that the cold atoms are alternately trapped and released, resulting in a pulsed operation of the cold atom source. On the other hand, manipulation of thermal atomic beams has been demonstrated with two-dimensional gradients having a zero-field axis along the atomic beam direction, resulting in high-brightness beams (10^9 atoms/s) at axial velocities ranging from a few m s^{-1} to a few tens of m s^{-1} in continuous operation [5–7].

In this paper, we present an experimental study of magneto-optical trapping in a two-dimensional magnetic field gradient as a possible starting point for a continuous beam of cold atoms operating from a thermal vapour. The 2D gradient MOT described in section 2 acts as a normal MOT in the horizontal plane and as a molasses without a position-dependent component of the force in the vertical direction. The main features of the experimental set-up

and techniques are briefly reviewed in section 2. In section 3, 3D and 2D gradient MOTs are compared for their capture efficiency and dependence on trapping parameters: field gradient and laser intensity. The moderate loss of capture efficiency in the anisotropic structure is well explained by the predicted angular dependence of the capture velocity. An interesting feature of anisotropic traps is that, as a result of the elongated shape of the cold atom cloud, multiple scattering of the cooling light is strongly reduced, leading to a significantly lower temperature than in an isotropic trap in comparable conditions. In the fourth section, measurements of the velocity induced by laser intensity imbalance and magnetic field, both in a 3D optical molasses and in the 2D gradient MOT are compared with theoretical estimates obtained from existing 1D and 2D models best approaching the experimental situation.

2. Experimental set-up and measuring methods

The experimental set-up has been described in detail elsewhere [8]. A specific feature of our MOT is the structure for the magnetic gradient. It consists of two independent ensembles of four straight conductors, respectively, parallel to the z and the y-axis, each producing a 2D quadrupole field (figure 1), that leaves the direction parallel to the wires free of a gradient. If both structures are operated at maximum current simultaneously, a 3D gradient equivalent to the anti-Helmholtz configuration is produced with a maximum x-component of 15 G cm^{-1}. With this set-up, isotropic and anisotropic traps can be studied. As a light source we use a laser diode spectrally narrowed in an extended cavity and frequency offset-

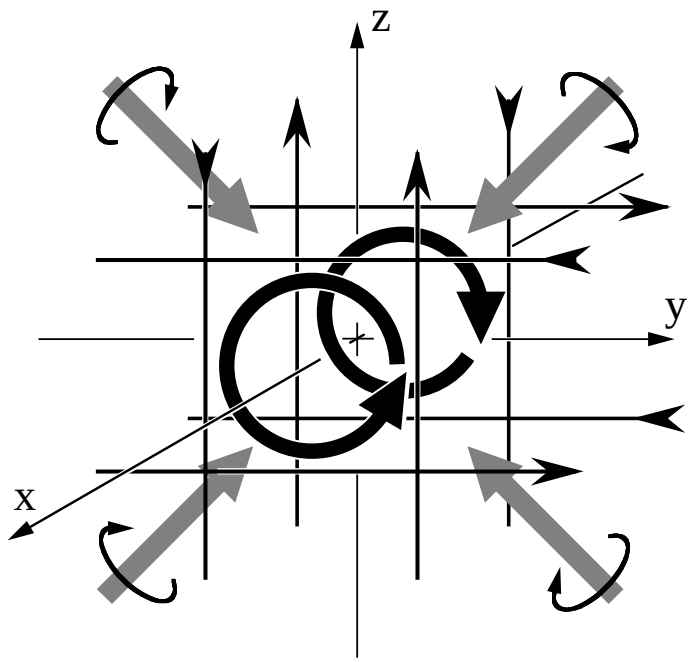

Figure 1. Scheme of the structure for the magnetic gradient and cooling beams geometry. Two independent ensembles of four straight wire conductors produce 2D quadrupole fields, respectively, in the (Oxy) and the (Oxz) plane. The two loops show equivalent anti-Helmholtz coils when both 2D gradients are on. Four cooling beams at 45° with respect to Oz lie in the (Oyz) plane. An additional two-beams pair along Ox is not shown.

locked to a saturated absorption cell. The required cooling power is obtained from a slave laser injection-locked to the extended cavity laser. The trap is irradiated by six independent laser beams with a $1/e$ diameter of 10 mm. Four beams are at 45° to the vertical z-axis in the (Oyz) plane and two run along the horizontal x-axis. All beams are circularly polarized according to the requirements of a magneto-optical trap. We load the trap directly from the caesium vapour present in the vacuum system. The repumping beam ($F = 3 \rightarrow F' = 4$) is mixed to one of the horizontal beams.

Temperature measurements. Temperature measurements are performed by the time-of-flight (TOF) technique. The 1 cm diameter probe laser beam is placed 25 cm below the trap. In a first step 10^7 atoms are captured in the magneto-optical trap in a loading time of about 1 s. For molasses measurements, the magnetic gradients are then switched off (fall time < 10 ms). The atoms thermalize in the optical molasses for an additional 5 ms before the cooling beams are cut off. This time has been found to be long enough to thermalize the atoms' velocity although the spatial distribution takes much longer to reach equilibrium. To analyse the temperature of the isotropic and the anisotropic trap, the magnetic fields are switched off 1 ms after the cooling beams. The acceleration due to the magnetic gradient alone during the two cut-offs does not affect the measured velocity distribution.

Drift velocity measurements. Two techniques are used to investigate the influence of a static magnetic field or an intensity imbalance on a molasses and an anisotropic trap. By measuring the TOF signal ($\mathrm{d}N/\mathrm{d}t$) one can easily calculate the initial distribution of velocity ($\mathrm{d}N/\mathrm{d}v_0$) along Oz. In all measurements, the measured drift velocities are smaller than the average velocity $\sqrt{2gh}$ gained by the free fall, resulting in a linear dependence of the initial velocity on the measured free-fall delay (1 cm s^{-1} (m s)$^{-1}$). We define an average drift velocity by

$$v_d = \frac{\int_{-\infty}^{+\infty} \frac{\mathrm{d}N}{\mathrm{d}v_0} v_0 \, \mathrm{d}v_0}{\int_{-\infty}^{+\infty} \frac{\mathrm{d}N}{\mathrm{d}v_0} \mathrm{d}v_0} \, . \tag{1}$$

The TOF method can be used for a molasses as well as for magneto-optical traps.

The second technique is specific to the anisotropic trap. It relies on the fact that the loss rate Γ_t of trapped atoms increases when atoms are extracted at an average velocity v_d. The loss rate is equal to the inverse of the loading time of the trap [9], which is as readily accessible experimentally as the total number of trapped atoms, N. However, the loading time only depends on Γ_t and gives a more direct measurement than N, which also depends on the capture rate and on its possible changes with the parameters that determine v_d.

In order to calculate the dependence of Γ_t on v_d, we assume that atoms are captured at an arbitrary, but uniform rate over the length L of the trap. A second assumption is that all atoms drift with the same average velocity v_d; it amounts to neglecting momentum diffusion, which is justified since the lifetime of the atoms in the trap (10^{-2}–1 s) is much longer than the momentum correlation time (~ 10 μs or less). Under these assumptions, the relation between loss rate and velocity is found to be

$$\Gamma_t(v_d) = \frac{\Gamma_c}{1 - (v_d/\Gamma_c L)(1 - \exp[-\Gamma_c L/v_d])} \simeq \begin{cases} v_d/L & \text{if} \quad v_d \ll \Gamma_c L \\ 2v_d/L & \text{if} \quad v_d \gg \Gamma_c L \end{cases} \tag{2}$$

where Γ_c is the collisional rate with thermal atoms. Using equation (2), the drift velocity is deduced from measurements of the loading time Γ_t^{-1} obtained by fitting the recorded transient fluorescence after trap turn-on with $(1 - \exp[-\Gamma_t t])$.

3. Capture efficiency, cloud shape and temperature

3.1. Capture efficiency

In this section, our goal is to compare the capture efficiency of an anisotropic magneto-optical trap to that of an isotropic one. In a previous work [8], we studied the capture process both theoretically and experimentally in an isotropic trap. We showed that under the assumption of its isotropy, a three-dimensional magneto-optical trap can be described by an entirely 1D model that takes into account the magnetic field gradient. Although most of the atoms enter the trap off-axis, it is shown that if typical 3D features—such as the power broadening due to the transverse beams and the mixing of the population of the Zeeman sublevels by the changing magnetic field and laser polarization—are taken into account, the capture process and the influence of the magnetic field on it may be described by considering the on-axis case only.

To make a theoretical comparison between the number of trapped atoms in the two configurations, we study the capture velocity in the Oxz plane using a 2D model [10]. In this plane both the isotropy and the anisotropy of the magnetic field can be easily modelled. With this 2D model we calculate for atoms moving towards the centre of the trap how the capture velocity depends on the angle between the velocity at the entrance of the trapping zone and the z-axis. The results of these calculations, shown in figure 2, indicate that in an isotropic trap the capture velocity depends only slightly on the incidence angle. On the other hand, in an anisotropic configuration the capture velocity decreases by about 20% as the direction of propagation of an atom changes from Ox (trapping axis) to Oz. From the results of figure 2, one can easily compute the capture rate of both traps [8]. With typical trapping conditions ($\delta = -2\Gamma$, $I = 2I_s$, $\mathrm{d}B_x/\mathrm{d}x = 10$ G cm^{-1}) the capture rate of an anisotropic trap is only 20% smaller than that of an isotropic one. If in both cases the losses are due to collisions between hot and cold Cs atoms [8, 9], one would expect the number of trapped atoms to be 20% smaller in the anisotropic configuration.

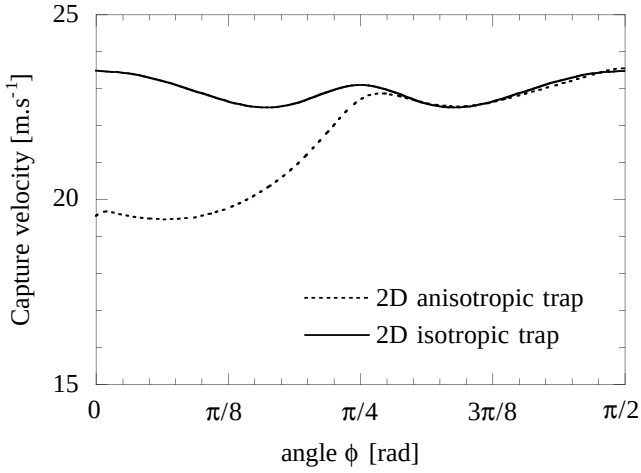

Figure 2. Calculated capture velocity versus angle between the velocity at the entrance of the trapping zone and the z-axis in the case of a 2D isotropic and anisotropic trap in the (Oxz) plane. For the anisotropic configuration Ox is the trapping axis. The trapping parameters are $\delta = -2\Gamma$, $I = 2I_s$ and $\mathrm{d}B_x/\mathrm{d}x = 10$ G cm^{-1}.

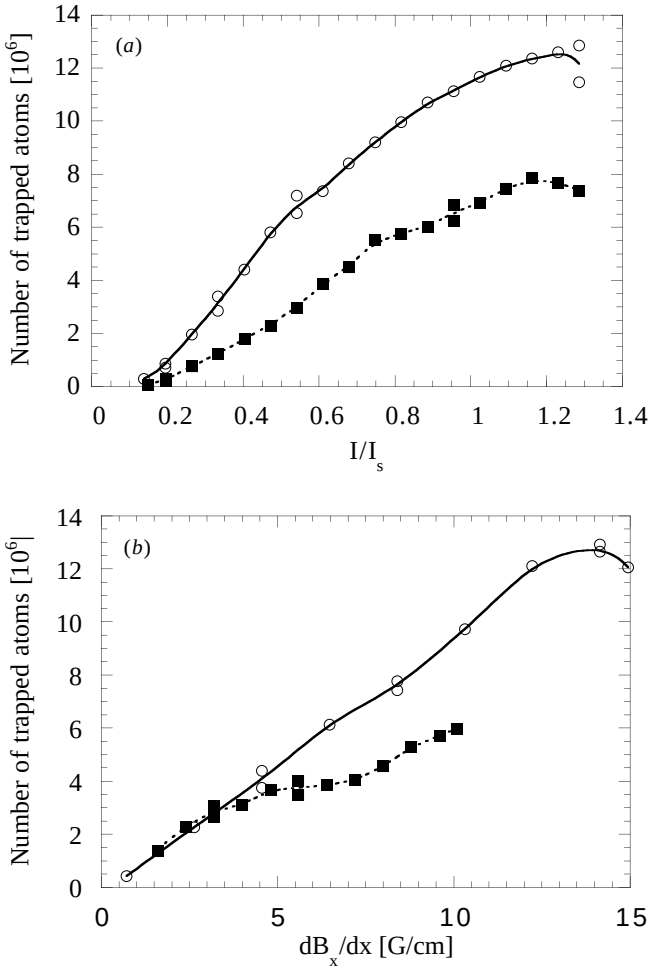

Figure 3. Comparison between the number of trapped atoms in a 2D and 3D gradient trap versus (*a*) cooling intensity and (*b*) the x-component of the magnetic field gradient. Open circles (○) represent the experimental results of the isotropic 3D trap, full squares (■) stand for those of the anisotropic 2D trap. For clarity the experimental values are joined by smoothed curves. For both graphs the detuning is held constant at -2Γ. In (*a*) $\mathrm{d}B_x/\mathrm{d}x = 10$ G cm, in (*b*) $I = 1.1 I_s$ where I is the intensity averaged over $1/\mathrm{e}^2$ and $I_s = 2.2$ mW cm^{-2}.

In addition, the 2D model shows that the number of atoms in the anisotropic trap depends on the magnetic gradient, the laser detuning and intensity in the same manner as in the isotropic trap.

Experimental data confirm these predictions. Figure 3(*a*) and (*b*) indicates that, for identical conditions of irradiation, the dependences of the number of trapped atoms on the laser intensity and the magnetic gradient are not modified when the magnetic field becomes anisotropic. This figure also shows that for the same value of $(\mathrm{d}B_x/\mathrm{d}x)$, the number of atoms in an anisotropic trap is about one half that of a spherical trap. This is somewhat lower than expected from the 2D model and can be explained as follows. In the anisotropic trap, the 1D $\sigma^+ - \sigma^-$ optical molasses presents a great sensitivity to imperfections such as local residual intensity imbalances (this is especially true during the capture process

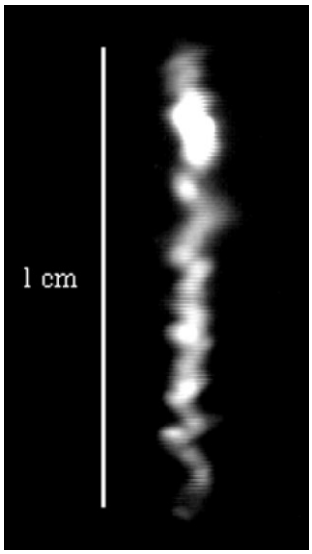

Figure 4. Image of a typical column of atoms in an anisotropic trap. The picture has been taken along the y-axis. The length of the cylindrical cloud is about 10 mm, its diameter is less than 1 mm.

where the Doppler regime dominates); these imperfections may lead to important atomic drift along this preferential direction. The loading time is identical in both geometries, indicating that the losses occur during the capture rather than by vertical diffusion of trapped atoms.

3.2. Elongated clouds of cold atoms

Figure 4 shows an elongated cloud of cold atoms in our anisotropic magneto-optical trap. The picture has been taken along the y-axis with a CCD camera. We observe a spurious structure in the cloud. First, one can see that the atoms are arranged in a 'furrow' that oscillates spatially in an irregular way around the vertical z-axis. The amplitude of these oscillations is of the order of 0.2–0.5 mm. Second, the atoms accumulate at several positions along the z-axis. Both features are hardly affected by a change of the cooling parameters such as laser detuning, intensity or relative phase of the laser beams. On the other hand they depend on the imperfections of the irradiation system such as laser misalignement, relative displacement of the beams or their unsmooth spatial profile. We conclude that the main reason for the observed structures is the local deviation from the Gaussian profile of the cooling beams. We tested this hypothesis by introducing an intensity imbalance between two counterpropagating beams of a trap. The observed displacement is in line with the predictions of a full quantum 2D model [11] and the measured deviations ($\sim$10%) from a Gaussian intensity distribution. The observed structures can considerably alter the directivity of a cold atom beam extracted from the anisotropic trap.

3.3. Temperature measurements

We investigated the cloud temperature in both optical molasses and magneto-optical traps. More particularly we have compared the values of an isotropic trap and the anisotropic situation as shown in figure 5: for these measurements, we changed the laser detuning and measured the number of trapped atoms while the laser intensity was kept constant. Our purpose is to determine the temperature of the traps for irradiation conditions close to

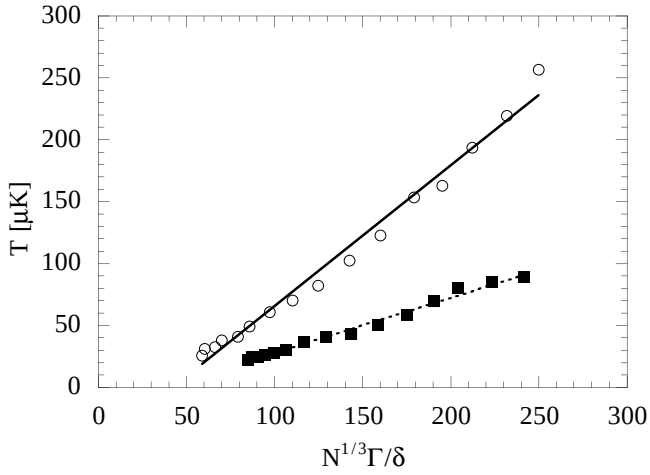

Figure 5. Temperature measurements in an isotropic trap (○) and an anisotropic trap (■) for different detunings. The cooling laser intensity is the same for all data ($I = 2\ I_s$).

those that optimize the capture process. The rather high temperatures that we obtain can be explained by the relatively strong laser intensity ($I = 2I_s$).

Plotted against the dimensionless parameter $N^{1/3}\Gamma/\delta$, the temperature of both traps show a linear law. As pointed out by Cooper *et al* [12], this linear dependence can be explained in terms of multiple scattering of photons. Moreover, the fact that the temperature of the anisotropic trap is lower than that of the isotropic one can also be understood within the multiple scattering picture. As shown by Cooper *et al*, the heating of atoms due to multiple scattering is proportional to the optical thickness $f = n\sigma l$ of the trap. Let us calculate the ratio between the optical thickness of the two traps. Let N_s, n_s (resp. N_a, n_a) be the number of trapped atoms and the density in the spherical (resp. anisotropic) trap: we define two coefficients α and β such as $N_a = \alpha N_s$ and $n_a = \beta n_s$. A simple calculation of the optical thickness ratio shows that

$$\frac{f_a}{f_s} = \left(\frac{1}{3}\pi^2\alpha\beta\frac{r_s}{L}\right)^{1/2} \tag{3}$$

where r_s is the radius of the spherical cloud and L the length of the elongated one. To obtain equation (3), it has been assumed that the angle-averaged diameter of the elongated cloud is given by $\bar{l}_a = \pi r_a$ where r_a is its radius. Equation (3) shows that for our experimental conditions ($L = 10$ mm, $r_s = 0.3$ mm and $\beta < 5$), $f_a < 0.5\ f_s$. This means that the heating due to multiple scattering of photons is significantly smaller in an anisotropic trap, in agreement with experimental data.

4. Drift velocities

4.1. Intensity imbalance

We measured the velocity of the drift induced by an intensity imbalance between up- and down-going beams, in an anisotropic trap and a 3D optical molasses. As in [13] the intensity imbalance is defined by the parameter $w = \frac{I_+ - I_-}{I_+ + I_-}$, where I_+ (resp. I_-) is the intensity of

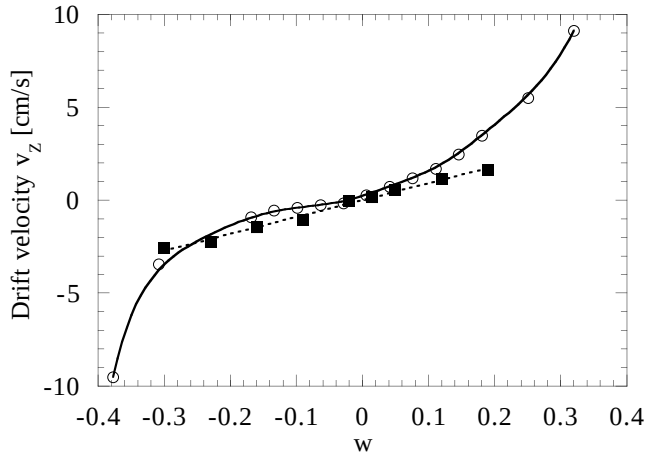

Figure 6. The drift velocity versus intensity imbalance w between up- and down-going beams. Open circles (○) represent the results of an anisotropic trap (loading time measurement), full squares (■) stand for the TOF measurements in a 3D molasses. For clarity the experimental values are joined by smoothed curves. The laser detuning and intensity per beam are given by $\delta = -3\Gamma$ and $I = 2I_s$.

the up- (resp. down-) going beams. We ensured that this measurements were not influenced by the residual static magnetic field in the trapping zone. The good agreement between these two velocities (see figure 6) shows that, as far as an intensity imbalance along Oz is concerned, the z-axis—free of trapping—of the anisotropic trap is equivalent to that of a 3D optical molasses. The presence of the transverse magnetic gradient does not alter the effect of an intensity imbalance along Oz. Also, this figure shows that the drift velocity is very small ($v_d \leqslant 2$ cm s^{-1}) for a wide range of imbalance. Such an insensitivity to intensity imbalance was known to be characteristic of sub-Doppler optical molasses [14]. Our measurements show that the transverse magnetic field in the 2D trap does not change the drift velocity induced by an intensity imbalance. In addition, the drift induced in a 2D trap exihibits a double slope. This double slope could not be observed in a 3D molasses because of the important decrease of the TOF signals when $|w| > 0.3$. To evaluate the potential for extracting atoms with an intensity imbalance, we represent in figure 7 the total number of atoms that cross the probe beam, when they are pushed away from the 3D molasses. This number, which corresponds to the integral of the TOF signal, decreases very quickly with increasing imbalance w. By measuring the number of trapped atoms, we found that the loss of signal is almost entirely due to the decrease of the capture efficiency induced by the intensity imbalance. The TOF signals do not show any broadening and are only slightly distorted for the extreme values of w.

4.2. Magnetic field

We also measured the drift velocity along the z-axis as a function of the static magnetic field (figure 8). The average velocities are 18 cm s^{-1} G^{-1} for 3D molasses, 18 cm s^{-1} G^{-1} for the anisotropic trap measured by the loading time and 22 cm s^{-1} G^{-1} for the anisotropic trap by the TOF method. The measured velocities are not significantly different, showing that the horizontal gradient field does not appreciably perturb the drift induced by the vertical, homogenous field. The same is true for the irregular density distribution, which is observed

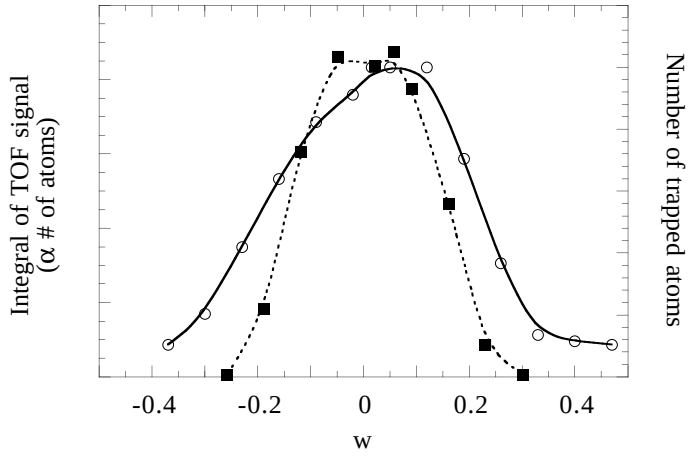

Figure 7. The integral of the TOF signal of an 3D molasses (○) and the number of trapped atoms (■) versus intensity imbalance w between up- and down-going beams. For clarity the experimental values are joined by smoothed curves. The laser detuning and intensity are given by: $\delta = -3\Gamma$ and $I = 2I_s$.

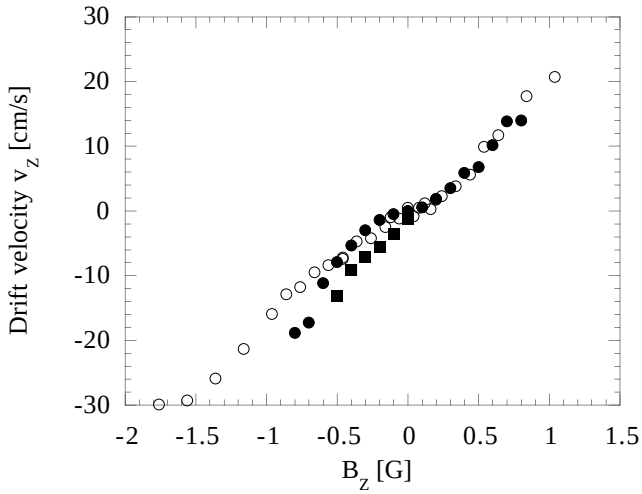

Figure 8. The drift velocitiy versus the static magnetic field B_z. The results of the anisotropic trap are represented with full symbols (■ for the TOF, ● for the loading time method), open circles (○) stand for the TOF measurements in a 3D molasses. The laser detuning and intensity are given by $\delta = -3\Gamma$ and $I = 2I_s$.

only in the 2D gradient trap. However, as shown in figure 10, the TOF signals are not only shifted along the time axis, they are also distorted and reduced in amplitude. In contrast with the case of the intensity imbalance, the loss of signal shown in figure 9 cannot be attributed to a decrease of the capture process efficiency: for $|B_z| = 1.5$ G, the number of trapped atoms is only 30% smaller than the number at $B_z = 0$ G. This shows that the drift velocity of the atoms also has non-vertical components. These effects already occur for very small values of the magnetic field ($B_z \sim 0.2$ G). In all cases the temperature is consistent with the sub-Doppler regime.

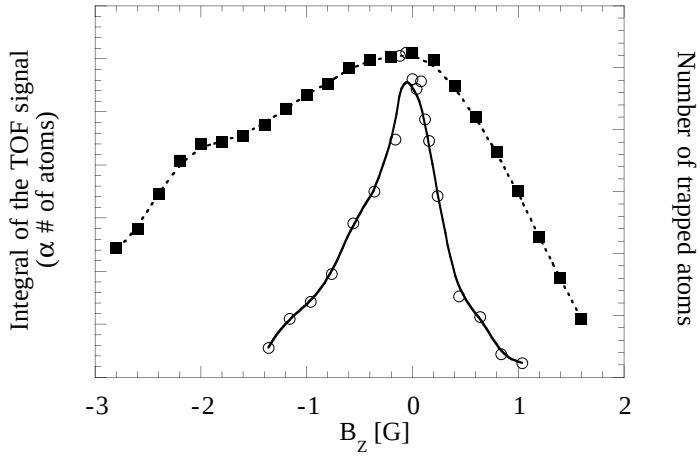

Figure 9. The integral of the TOF signal of a 3D molasses (○) and the number of trapped atoms (■) versus vertical magnetic field B_z. For clarity the experimental values are joined by smoothed curves. The laser detuning and intensity are given by $\delta = -3\Gamma$ and $I = 2I_s$.

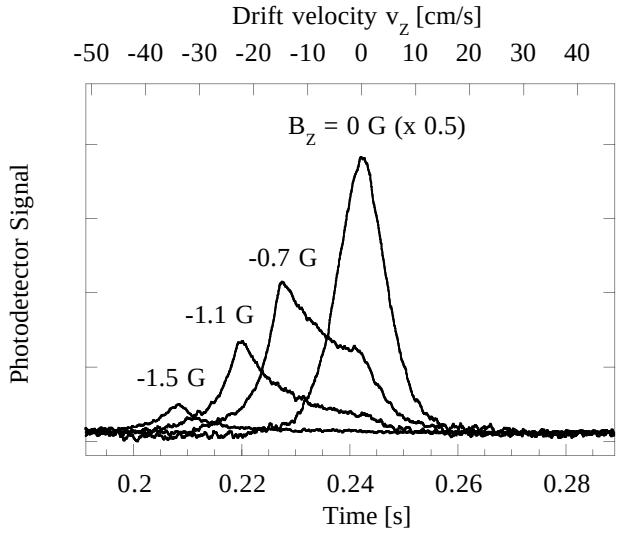

Figure 10. TOF signals of a 3D molasses for different static magnetic fields along the vertical z-axis. The signal for B_z = 0 is divided by a factor of 2. The arrival time of the atoms having an initial velocity $v_0 = 0$ is 242 ms. By an initial velocity of 1 cm s^{-1} the arrival time changes by 1 ms. The laser detuning and intensity are given by $\delta = -3\Gamma$ and $I = 2I_s$.

5. Discussion

5.1. Theoretical predictions

In order to understand qualitatively our experimental results, we developed a theoretical 1D model using the transition $J = 1 \rightarrow 2$ to study the effect of both intensity imbalance and longitudinal magnetic field on a $\sigma^+ - \sigma^-$ molasses. We are aware that our experimental situation cannot be fully described by this simple 1D model. Our purpose, here, is to point

out among all the experimental features those which can be easily understood. Using the procedure described by Dalibard *et al* [15], we calculate the cooling force at small laser intensity for any value of the atomic velocity, while taking into account the modifications in the atomic density matrix induced simultaneously by an intensity imbalance or a magnetic field. As already predicted by Werner *et al* [16] for an intensity imbalance and by Walhout *et al* [17] for the magnetic field, the net effect of such a perturbation is to shift the velocity for which the force vanishes to a non-zero value. This model allows us to distinguish two different regimes of drift. The first one corresponds to small values of intensity imbalance ($w \ll 1$) and magnetic field ($\mu_B g_g B \ll \hbar\Gamma'$, where $g_g = 0.25$ is the Landé factor of the Cs ground state, μ_B is the Bohr magneton and Γ' is the rate of optical pumping). This is the sub-Doppler regime: for our cooling parameters, the velocities of the drift induced by an intensity imbalance w and a magnetic field B are then given by

$$\left(\frac{kv_d}{\Gamma}\right)_w^{SD} = -\frac{1}{3}\frac{\Gamma}{\delta}\frac{I}{I_s}w \tag{4}$$

$$\left(\frac{kv_d}{\Gamma}\right)_B^{SD} = \frac{g_g\mu_B B}{\hbar\Gamma} \tag{5}$$

where k, δ, I are the wavenumber, the detuning and the intensity of the cooling beams, respectively; $I_s = 2.2$ mW cm^{-2} is the intensity for which the Rabi angular frequency is equal to Γ for the $|F = 4, m_g = 4\rangle \rightarrow |F' = 5, m_e = 5\rangle$ transition. For higher values of the imbalance ($w > 0.3$) and the magnetic field ($\mu_B g_g B > \hbar\Gamma'$) the regime becomes Doppler and the drift velocities are then given by

$$\left(\frac{kv_d}{\Gamma}\right)_w^{D} = -\frac{\delta}{2\Gamma}w \tag{6}$$

$$\left(\frac{kv_d}{\Gamma}\right)_B^{D} \simeq \frac{g_e\mu_B B}{\hbar\Gamma} \tag{7}$$

where $g_e = 0.4$ is the Landé factor of the Cs excited state. Let us also point out that for intermediate values of the intensity imbalance ($w \sim 0.3$) and the magnetic field ($\mu_B g_g B \sim \hbar\Gamma'$), the force vanishes for three different values of the velocity. By solving the corresponding Fokker–Planck equation, one can show [16, 17], that the velocity distribution is no longer Gaussian: it becomes a distribution with two peaks more or less resolved.

For weak intensity imbalances ($w \ll 1$), Werner *et al* [16] calculated that the drift velocity using a $F = 4 \rightarrow 5$ transition is eight times smaller than that given by equation (4). We use this factor to obtain the imbalance drift coefficient in cell B3 of table 1 from cell B2. The boundaries between the Doppler and sub-Doppler regimes as w and B vary are not known in the $F = 4 \rightarrow 5$ case.

As mentioned by Steane *et al* [13] and Werner *et al* [16] a more complete description must take into account the three-dimensional character of the cooling and the real atomic transition involved (i.e. $F = 4 \rightarrow 5$). Such a model was developed by Castin *et al* [18] using the so-called Monte Carlo wavefunction technique to calculate the effect of an intensity imbalance and a static magnetic field on a 2D optical molasses. These fully quantum mechanical calculations were made with cooling parameters ($\delta = -3\Gamma$, $I = I_s$) close to our experimental conditions. Its results are shown in row 4 of table 1.

In order to compare the experimental results with the available theoretical predictions it is also useful to recall the characteristics of the cooling beam geometries involved. All theoretical predictions are made for drift velocities along one pair of σ^+–σ^- polarized beams ($\boldsymbol{k} \parallel Oz$), the drift velocity being induced either by unequal intensities or by a

Table 1. Summary of the theoretical and experimental drift-induced velocities.

		A v_d/B (cm s^{-1} G^{-1})		B v_d/w (cm s^{-1})
	Doppler 1D model			
1	$\delta = -3\Gamma$	48		680
	Sub-Doppler 1D model			
2	$J = 1 \rightarrow J' = 2$ $\delta = -3\Gamma$, $I = 2I_s$	29		87.4
	Sub-Doppler 1D model			
3	$F = 4 \rightarrow F' = 5$ $\delta = -3\Gamma$, $I = 2I_s$	29		11
	2D quantum model			
4	$F = 4 \rightarrow F' = 5$ $\delta = -3\Gamma$, $I = I_s$	18		21
	Experiment 3D molasses			
5	$\delta = -3\Gamma$, $I = 2I_s$	TOF mean velocity	18	9
	Experiment			
6	Anisotropic trap $\delta = -3\Gamma$, $I = 2I_s$	Loading time TOF mean velocity	18 22	9 ($\lvert w\rvert < 0.25$)

magnetic field B_z. In 2D molasses calculations, the additional pair of beams propagating along Oy adds two plane standing waves polarized linearly parallel to Ox (σ_x) and Oz (π), respectively. In our experimental configuration the two pairs of beams are rotated around Ox by 45°, giving rise to the same three components: a $\sigma^+ - \sigma^-$ pair propagating along $\pm Oz$, and two standing waves of σ_x and π polarizations. An important difference between the two configurations is that the wave vectors along Oy and Oz which are equal to $k = 2\pi/\lambda$ in the 'straight' configuration, become $\bar{k} = k/\sqrt{2}$ in the 45° configuration. As a consequence, the sub-Doppler drift velocities predicted for a straight configuration (equations (4) and (5)) are expected to be $\sqrt{2}$ higher in 45° beams, so that rows 2 to 4 of table 1 should be multiplied by $\sqrt{2}$ in order to apply to the present experimental situation.

5.2. Effect of an intensity imbalance

The experimental values (cells B5 and B6 of table 1) agree with each other and lie significantly lower than any of the theoretical predictions for small values of the relative imbalance ($w < 0.25$) (9 cm s^{-1} for $w = 1$ as compared to $11\sqrt{2} = 15$ cm s^{-1} for the 1D sub-Doppler model and $21\sqrt{2} = 30$ cm s^{-1} for the 2D quantum model). We verified experimentally that, as described by equation (4), the drift coefficient increases with increasing saturation parameter I/I_s. For $w > 0.25$, the drift velocity in the anisotropic trap increases rapidly. The velocities are still too small to result from Doppler processes, but the behaviour of the curve would suggest the onset of such a regime. The range of w values where the transition from sub-Doppler to Doppler regimes takes place is consistent with numerical calculations made (for $\delta = -4\Gamma$ and $I = I_s/4$, however) by Werner *et al* [16] on the $F = 4 \rightarrow 5$ Cs transition. The transition observed near $w = 0.25$ also coincides with a sharp drop in the number of trapped atoms and in the total number of atoms detected in the TOF measurements in figure 7, which are both due to a loss of atoms during their capture phase.

5.3. Effect of the magnetic field

As shown in cells A5 and A6 of table 1, the experimental drift velocity (18–22 cm s^{-1} G^{-1}) induced by a vertical magnetic field on an optical molasses or an anisotropic trap is significantly lower than the $29\sqrt{2} = 41$ cm s^{-1} predicted by the 1D sub-Doppler model [19]. This discrepancy can be explained by the effect of additional laser beams which carry other polarization components than the $\sigma^+-\sigma^-$ configuration of the 1D model. This reduces the anisotropy created by the optical pumping which is at the origin of the orientational cooling mechanism [15]. The fully quantum mechanical computation of Castin [11] indeed predicts such a reduction (cell A4 of table 1) and is in reasonable agreement with the measured values.

1D models of magnetic-field-induced drift predict, as in the case of an intensity imbalance, a double-peaked velocity distribution in the intermediate range of magnetic field. The distorted velocity distribution in the TOF signals of figure 10 cannot, however, be explained in such terms: the full spread is too small to originate from Doppler processes. In addition, a comparison with experimental results on the effect of a longitudinal magnetic field on a 1D molasses [19] shows that, in the range of magnetic field considered in our experiment, the drift velocity arises exclusively from sub-Doppler mechanisms. We believe that the distortion of the TOF signals is mainly due to the presence of small local potential wells in the z direction. At small magnetic fields a part of the atoms is held in these potential wells and does not acquire any drift velocity. As can be seen from figure 10, the fraction of these atoms decreases if the magnetic field is increased. As already pointed out, a multiple-beam $\sigma^+-\sigma^-$ molasses adds a structure of two-dimensional standing waves to the $\sigma^+-\sigma^-$ molasses. The potential wells due to light shifts are periodic in the drift (Oz) direction as well as in the horizontal directions. The atoms trapped in these wells may account for the side peak near $v = 0$ in the TOF spectra of figure 10. The depth of the potential wells is proportional to E^2/δ, where E^2 is the square of the total electric field due to the laser beams. As an estimate of the potential well depth, we calculate the modulation

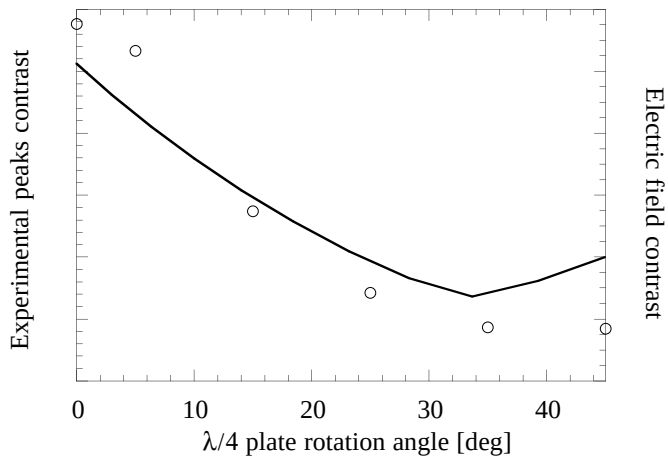

Figure 11. Open circles (○), ratio of $v = 0$ to $v \neq 0$ peak heights in the TOF spectra of 3D molasses in a vertical magnetic field versus ellipticity of the four (Oyz) cooling beams ($0^\circ \rightarrow$ lin ∥ lin; $45^\circ \rightarrow \sigma^+-\sigma^-$). Full curves, average depth (in the Oz direction) of potential wells, estimated by the peak-to-valley difference of E^2, averaged over y and over the relative phase of the two 45° molasses beam pairs.

amplitude ΔE^2 of $E^2(y, \phi)$ along Oz (ϕ is the relative phase between the two beam pairs). The depth of the wells for atoms travelling in the Oz direction is then an average of ΔE^2 over y and ϕ. The resulting average is plotted in figure 11 as a function of the ellipticity of the polarization of the four beams. The measured relative number of atoms at $v = 0$ is in good qualitative agreement with the estimated well depth.

As far as the continuous extraction of atoms is concerned, our measurements indicate that the drift induced by a vertical magnetic field with two pairs of beams at 45° with respect to the z-axis, does not depend on the magnetic field in such a simple way as in the 1D configuration where the applied field is parallel to the pair of laser beams. The usefulness of the magnetic field for extracting atoms from an anisotropic trap is thus restricted to a moderate range of magnetic fields ($B \leqslant 0.2$ G) and velocities ($v_d \leqslant 10$ cm s^{-1}).

6. Conclusion

We have investigated an anisotropic magneto-optical trap as a potential tool for producing a continuous beam of laser-cooled atoms. We studied the capture efficiency and the cloud temperature as a function of the cooling parameters and compare the results with values of the isotropic situation. The anisotropic trap shows a capture efficiency which is typically one half that of an isotropic trap. The temperature of the elongated clouds is found to be lower than the temperature in 3D traps. This difference can be explained in terms of excess heating due to multiple scattering of photons between laser-cooled atoms, which is expected to be higher in an isotropic cloud of cold atoms than in an anisotropic one.

We further examined an intensity imbalance and a static magnetic field as means for extraction of atoms from an anisotropic trap. We demonstrate that atoms can be pushed out of such a structure using these two methods. However, the low sensitivity of sub-Doppler molasses to intensity imbalance yields some obstacles for this method to produce velocities of the order of tens of cm s^{-1}. A static magnetic field is more likely to induce such velocities to atoms cooled in a anisotropic trap. The measured drift coefficient is slightly lower than the 1D prediction but is in agreement with a full quantum 2D calculation.

Other drift mechanisms such as moving molasses, in possible combination with dark channels, are promising alternatives to the simple methods described here and will also be investigated.

Acknowledgments

This work was supported by the Swiss National Science Foundation and the Federal Office of Metrology. The authors wish to thank Y Castin for providing theoretical results on 2D molasses.

References

[1] Raab E L, Prentiss M, Cable A, Chu S and Pritchard D E 1987 *Phys. Rev. Lett.* **59** 2631
[2] Townsend C G, Edwards N H, Cooper C J, Zetie K P, Foot C J, Steane A M, Szriftgiser P, Perrin H and Dalibard J 1995 *Phys. Rev.* A **52** 1423
[3] Steane A M and Foot C J 1991 *Europhys. Lett.* **14** 231
[4] Drewsen M, Laurent Ph, Nadir A, Santarelli G, Clairon A, Castin Y, Grison D and Salomon C 1994 *Appl. Phys.* B **59** 283
[5] Nellessen J, Werner J and Ertmer W 1990 *Opt. Commun.* **78** 300
[6] Riis E, Weiss D S, Moler K A and Chu S 1990 *Phys. Rev. Lett.* **65** 1658
[7] Yu J, Djemaa J, Nosbaum P and Pillet P 1994 *Opt. Commun.* **112** 136

[8] Sagna N, Dudle G and Thomann P 1995 *J. Phys. B: At. Mol. Opt. Phys.* **28** 3213
[9] Monroe C, Swann W, Robinson H and Wieman C 1990 *Phys. Rev. Lett.* **65** 1571
[10] Sagna N 1996 *PhD Thesis* Université de Neuchâtel
[11] Castin Y unpublished
[12] Cooper C J, Hillenbrand G, Rink J, Townsend C G, Zetie K and Foot C J 1994 *Europhys. Lett.* **28** 397
[13] Steane A M, Chowdhury M and Foot C J 1992 *J. Opt. Soc. Am.* B **9** 2142
[14] Lett P D, Phillips W D, Rolston S L, Tanner C E, Watts R N and Westbrook C I 1989 *J. Opt. Soc. Am.* B **6** 2085
[15] Dalibard J and Cohen-Tannoudji C 1989 *J. Opt. Soc. Am.* B **6** 2023
[16] Werner J, Hillenbrand G and Steane A 1993 *J. Phys. B: At. Mol. Opt. Phys.* **26** 3063
[17] Walhout M, Dalibard J, Rolston S L and Phillips W D 1992 *J. Opt. Soc. Am.* B **9** 1997
[18] Castin Y and lmer K M 1995 *Phys. Rev. Lett.* **74** 3772
[19] Valentin C, Gagné M-C, Yu J and Pillet P 1992 *Europhys. Lett.* **17** 133